On Copernicus DEM - DTM and ICESat for height and biomass retrieval of tropical forests

Citation for the original published paper (version of record):
Askne, J. (2026). On Copernicus DEM - DTM and ICESat for height and biomass retrieval of tropical forests. IEEE Journal of Selected Topics in Applied Earth Observations and Remote Sensing, In Press. http://dx.doi.org/10.1109/JSTARS.2026.3722731

(article starts on next page)

This article has been accepted for publication in IEEE Journal of Selected Topics in Applied Earth Observations and Remote Sensing. This is the author's version which has not been fu
content may change prior to final publication. Citation information: DOI 10.1109/JSTARS.2026.3722731

On Copernicus DEM – DTM and ICESat for height and biomass retrieval of tropical forests.

Jan I.H. Askne, *Fellow, IEEE* Scopus Author ID: 7006850123

***Abstract*— The Copernicus DEM – DTM difference was shown by Soja et al in [1] to be linearly correlated with above ground biomass, AGB, for eleven test sites with a resolution of about 30 m for the Copernicus DEM and 100 m for the DTM. The goal of this paper is to give a model to explain why this is caused by both variables being dependent on the product of forest density and height. An expression representing the mean of TanDEM-X phase heights or Copernicus DEM – DTM according to the Interferometric Water Cloud Model (IWCM) is used to estimate canopy height, area-fill (canopy cover), and AGB, the latter with and without 5% training data. The IWCM area-fill is determined using an ICESat-type approach [2], introducing a parameter q0, determined by the geolocation of the site, to quantify the height-density relationship. The analysis is conducted based on the data from [1] using LVIS lidar observations from the TropiSAR and AfriSAR sites and ALS data from the BIOSAR sites (Krycklan and Remningstorp) and various methods from three additional sites, altogether from four continents. Results indicate an almost linear relationship, between mean phase height, IWCM mean canopy height, and AGB. For the boreal sites, the relative RMSE is comparatively high, whereas for the tropical sites the relative RMSE is around 14% for mean canopy height and 11-18 % for the tropical sites but for Mondah (31%) for AGB in line with [1]. The lower RMSEr for sites with larger forest mean heights is mainly associated with a relatively constant Copernicus DEM vertical error. The almost linear relation between mean values of the Copernicus DEM – DTM difference and the mean AGB with r^2=0.97 demonstrates the feasibility of AGB retrieval without local calibration, tested on three temperate sites on two continents. All results are based on the availability of a DTM, which is expected from BIOMASS.**

***Index Terms*— Above-ground biomass, forest height, forest structure, interferometric synthetic aperture radar, Copernicus DEM, DTM, Interferometric Water Cloud Model.**

I. INTRODUCTION

ABOVE ground biomass (AGB), defined here as biomass density per unit area (Mg/ha), is important to investigate, e.g. [1] [2] as one of the 55 Essential Climate Variables (ECVs) specified by the Global Climate Observing System, and is fundamental for quantifying climate system change [3].

Remote sensing systems do not directly measure AGB, which depends not only on forest structure but also on wood density, and therefore requires in situ information on wood density linked to tree species. Nonetheless, linear relationships between the product of basal area and height and AGB—or non-linear formulations linking canopy height to AGB—have proven effective when calibrated with site-specific coefficients e.g. [4].

Airborne laser scanning (ALS) represents the most accurate remote sensing method for AGB estimation, although it is constrained by limited spatial coverage and comparatively high acquisition costs. ALS data are frequently used, together with in situ measurements, as reference for satellite-based investigations. ALS, AGB and stem volume have been related to canopy density and height e.g. [5] [6]. Extensive ALS-based studies e.g. [7] have enabled the development of satellite lidar missions e.g., [8] [9]. Lidar measurements of vertical forest structure are closely linked to AGB and are commonly parameterized using height percentile metrics [9], which themselves are sensitive to canopy density [10].

The launch of ERS-1 in 1991 demonstrated that C-band backscatter from forests is highly variable due to meteorological effects; however, 3-day interferometric coherence was shown to be sensitive to stem volume in meteorologically stable conditions [11] [12]. This resulted in the formulation of the Interferometric Water Cloud Model (IWCM) [13], describing interferometric height and density dependencies. In general, lower microwave frequencies (P-band) exhibit increased sensitivity to biomass relative to X- and C-band due to deeper canopy penetration, enabling interaction with stems and large branches e.g., [14] [15] [16]). ESA's P-band BIOMASS mission, launched in 2025, is designed to provide critical forest biomass estimates together with a global digital terrain model (DTM).

Higher-frequency systems have also proven useful. Meteorologically induced variation in C-band backscatter has been mitigated using multi-temporal processing, and long-term continuity from ESA's C-band SAR satellites has produced an extensive temporal data record [17] [18] [19]. The CCI BIOMASS project now provides spatially explicit AGB estimates for five epochs, although C-band backscatter sensitivity to biomass remains limited in tropical forests.

A major advance in SAR interferometry was achieved with

Jan I.H. Askne is with the Department of Environmental and Energy Sciences Chalmers University of Technology, SE-412 96 Gothenburg Sweden (e-mail: jan.askne@chalmers.se jan.askne@gmail.com).

Color versions of one or more of the figures in this article are available online at http://ieeexplore.ieee.org

SRTM [20] and TanDEM-X [21], which provide acquisitions without temporal decorrelation and stable phase-height estimates (phase height is defined as the average elevation of a InSAR- based DEM above a ground surface). When combined with a DTM, the interferometric phase height provides canopy height after model-based correction for penetration. Numerous studies have demonstrated the utility of TanDEM-X for forest characterization. Early work on tropical biomass estimation used TanDEM-X coherence [22], followed by investigations using TanDEM-X phase height variations for biomass variation [23].

Tropical forests contain a major fraction of global biomass, yet uncertainty remains substantial. Estimating AGB in tropical regions—often obstructed by persistent cloud cover—remains a high priority. Although low-frequency systems have been emphasized, trunk–ground scattering complicates interpretation. Tomographic SAR (TomoSAR) approaches have shown strong correlation between the scattering at ≈30 m height and AGB e.g. [24] [25]). However, TomoSAR is technically complex and is based on airborne experimental evidence from a limited number of sites. The method implemented in the prototype BIOMASS ground processor is derived after ground cancellation [26] [27], e.g. using the semi-empirical RVoG model [28] [29], and purely volume-only components correlate with AGB at $r^2 \approx 0.73$, giving RMSEr ≈ 20% across AfriSAR and TropoSAR [26]. The long wavelength of P-band means that the influence of canopy cover is of lower importance.

The goal of this paper is to investigate the physical reason for the correlation between the high-resolution Copernicus DEM and a DTM and AGB by means of IWCM. Models explaining the relation are important for application in relatively unknown areas.

The reminder of the paper is structured as follows: The available satellite data are described, followed by test sites and their properties. The model analysis is presented and forest height is derived. AGB is derived using 5% of the observations for training for boreal and tropical sites. The results are related to available ICESat data [2]. Finally, the results are applied on three temperate sites on two continents without the use of training and the results are discussed and conclusions drawn.

II. Data [1]

A. TanDEM-X

TanDEM-X is the German formation-flying two satellite system with X-band synthetic aperture radar, SAR, launched in 2010. The primary objective of the mission is to achieve a global Digital Elevation Model, DEM, with 12 m horizontal and 2 m vertical resolution [30] [31]. Since the radar only partly penetrates into a forest layer the DEM includes the effect of vegetation. With a digital terrain model, DTM, from other sources, the effect of the vegetation layer can be determined, and a phase-height can be obtained indicating the forest height minus the penetration of the microwaves. With IWCM the penetration can be estimated and the height is retrieved. The sensitivity of the phase-height to the microwave penetration is related to certain forest properties and to the height of ambiguity, HoA, related to the distance between the two satellites which varies between the acquisitions. For this reason, the DEM is based on acquisitions with varying HoA values. For the TanDEM-X DEM, HoA values of the order 35 and 45 m were generally chosen for obtaining high accuracy of reasonable topography, but for areas covered by forest (which can be determined from the TanDEM-X coherence) where the X-band wave partly penetrates and are scattered from different heights, a higher HoA is needed. For forest areas the phase height is also dependent on properties sensitive to meteorological conditions, which affects the scattering. This means that averaging of different acquisitions to obtain the TanDEM-X DEM is needed to minimize this environmental influence. The DEM, after correction with a known DTM, then represents a mean phase height of a number of acquisitions for which an expression can determined by means of the semi-empirical IWCM, e.g. [32].

B. Copernicus DEM

The GLO-30 version of the Copernicus DEM, which has a resolution of about 30 m is used in this paper based on data from Soja et al [1]. Information indicates that, for each test site, more than 97 % of the Copernicus DEM pixels over forests originated from InSAR data, of which more than 92 % originated from TanDEM-X data while the rest mainly from SRTM. Depending on the test site, between three and thirteen TanDEM-X acquisitions were acquired during the 2010–2015 global mapping campaign, predominantly in unfrozen, leaf-on conditions. For all test sites, the average temporal offset between the DEM and AGB reference data was below five years.

C. DTM

DTMs derived from airborne lidar data were available for all test sites at resolutions of 0.5–2 m from which a coarse resolution DTM is generated. In the future, BIOMASS is supposed to determine a DTM with a resolution of ca. 100 m×100 m and within an accuracy estimated to an RMS error of 3 meters [33] [34].

D. ICESat

ICESat is a NASA Iidar satellite for measuring, among other aspects, vegetation characteristics between 2003 and 2009 with close to global coverage. It has a footprint of 65 m diameter spaced 172 m along track and provides the relationship between canopy density and canopy height, shown in [2] to vary across forest types (biomes) described by a single parameter, q0, and the area-fill factor in IWCM corresponding to ALS vegetation ratio is expressed as

$$\eta(q0, h) = 1 - e^{-q0 \cdot h} \quad (1)$$

The factor q0 varies between different forest types in a world-wide investigation [2]. In the present paper the product $\eta(q0, h)h$ will be of particular interest, and this product does not vary very much for a slight change of q0 as illustrated in Fig. 1.

This means that the error associated with a q0 value typical for the forest types as illustrated in [2] rather than for the specific site investigated will not be very large, and when combined with TanDEM-X phase height the lower resolution of ICESat is not expected to be a problem. We will use the q0 value as a certain characteristic of the forest types studied, see [2] [35].

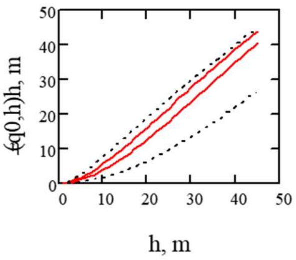

Fig. 1. Relation between η(q0,h)h and h with q0 varying for values typical for biomes [2}, q0=0.051 – 0.083 (red solid), but also extremes (black dotted).

III. Test sites

Krycklan (Lat 64° 16' N, Long. 19° 46' E) is a river catchment in northern Sweden, covering approximately 6800 hectares in the boreal zone. The forest is predominantly composed of Norway spruce (Picea abies (L.) Karst.), Scots pine (Pinus sylvestris L.), and birch (Betula spp.). The ground elevation is ranging from 145 m to 400 m above sea level. The test site is managed by various owners and management philosophies and serves as a research site for the Swedish University of Agricultural Sciences. It featured the ESA field campaign, BIOSAR 2008 [36].

Remningstorp (Lat. 58° 30' N, Long. 13° 40' E) is an estate with 1200 hectares forest area in the hemi-boreal zone, mainly composed of Norway spruce (Picea abies (L.) Karst.), Scots pine (Pinus sylvestris L.), and birch (Betula spp.). The site is relatively flat, with elevations ranging from 120 to 145 m above sea level. It also serves as a research site for the Swedish University of Agricultural Sciences, SLU, and was part of the ESA field campaign, BIOSAR 2010 [37].

The tropical sites studied here are from the ESA AfriSAR and TropiSAR experiments [38] with detailed in situ data, and referred to for more detailed information. The forest inventories in Lopé, Mondah, Mabounie, and Rabi were carried out in the AfriSAR 2016, and the inventories in Nouragues and Paracou were carried out in the TropiSAR 2009.

Lopé (Lat. 0.20° S, Long 11.59° E) is located in the Lopé national park, a UNESCO World Heritage in Gabon. Topography is gently hilly and vegetation is a forest-savanna mosaic with different forest types. There are on an average 35 tree species richness per ha, with high disparities between savanna and forest as well as between forest types. [6].

Mondah (Lat. 0.57° S, Long. 9.35° E) has a maritime climate, different vegetation types including Aucoumea-dominated forests and mixed forests of varying heights [39]. Mean tree species richness is similar to that in Lopé. There are on an average 35 tree species richness per ha, varying vegetation types. The proximity to Libreville creates anthropogenic effects.

Mabounié (Lat. 0.76° S, Long. 10.56° E) Altitude ranges between 25 and 230 m asl. There are typically about 55 tree species per ha.

Rabi (Lat. 1.93° S, Long. 9.88° E) Altitude ranges between 30 and 80 m asl. About 85 species per ha. dominated by lowland tropical rainforest.

Nouragues: (Lat. 4.06° N, Long 52.68° W) is located ca. 100 km south of Cayenne, French Guiana. The area is under total protection since 1996. High-canopy old-growth forest, and lower-canopy forest are included in the area.

Paracou: (Lat 5.27° N, Long 52.93°W) is located ca. 75 km West of Cayenne. It is a rain forest with a mean tree species richness of 140 per ha, comparable to that in Nouragues, the site is dominated by moist evergreen rainforest.

Three temperate sites on two continents will be included as examples on estimating biomass without training points:

Białowieża (Lat 23.69°°E, Long 52.72˚N): Multi-species forest stands, partially of natural origin, and partially comprising the primaeval forest (Białowieża National Park). The area is dominated by oak, beech, spruce, and pine, and has experienced significant bark beetle infestation since 2012 [40]

Kermeter (Lat 6.45°E, Long 50.61°N): Located within Eifel National Park, this site is ecologically diverse, with dominant species including beech, oak, and spruce [41].

Warra (Lat 146.65°E, Long 43.11°S): Characterized by tall lowland Eucalyptus obliqua forests with dense, multi-layered understories composed of wet sclerophyll and rainforest species. The site suffered significant damage during the 2019 bushfires [42].

We have then representatives of the major types of forests.

IV. Model

To interpret the TanDEM-X phase height data IWCM can be used. It is based on the assumption how the forest height as well as density is influencing the interaction with microwaves at X- and C-band [13] [43] [44] due to the small wavelength and the potential to penetrate gaps in the canopy. Using IWCM, an expression for the phase height and its dependence on the attenuation back and forth through the forest layer, α Np/m, and the scattering from the forest σ_{veg}^0 and the ground σ_{gr}^0, or rather the ratio $m = \sigma_{gr}^0/\sigma_{veg}^0$, can be obtained. From the expressions for the volume decorrelation, $\tilde{\gamma}_{vol}$, the complex correlation $\hat{\gamma}$,

This article has been accepted for publication in IEEE Journal of Selected Topics in Applied Earth Observations and Remote Sensing. This is the author's version which has not been fu
content may change prior to final publication. Citation information: DOI 10.1109/JSTARS.2026.3722731

the phase height, PhIWCM, is determined [32].

$$\tilde{\gamma}_{vol} = \frac{\int_0^h e^{-\alpha(h-z')} \cdot e^{-j\frac{2\pi}{HoA}z'} dz'}{\int_0^h e^{-\alpha(h-z')} dz'} = \frac{\alpha}{\alpha - j\frac{2\pi}{HoA}} \left(e^{-j\frac{2\pi}{HoA}h} - e^{-\alpha h}\right) \frac{1}{1-e^{-\alpha h}} = \gamma_{vol} e^{-j} \tag{2a}$$

$$\hat{\gamma} = \gamma_{sys} \frac{\tilde{\gamma}_{vol} + M}{1+M}, \text{ where } M = m \frac{\frac{1-\eta}{\eta} + e^{-\alpha h}}{1-e^{-\alpha h}} \text{ and } m = \frac{\sigma_{gr}^0}{\sigma_{veg}^0} \tag{2b}$$

$$PhIWCM = -\frac{HoA}{2\pi} \arg(\hat{\gamma}) = -\frac{HoA}{2\pi} \left[\varphi - atan\left(\frac{\sin(\varphi)}{\frac{\gamma_{vol}}{M} + \cos(\varphi)}\right) + n \cdot 2\pi\right] \tag{2c}$$

[the minus sign is related to the exp($-j\frac{2\pi}{HoA}z$)-assumption, and n to the possible phase shifts]. PhIWCM is a function of α, m, HoA and n, where n is the branch of solutions. When $\frac{2\pi}{\alpha HoA} \ll 1$ and exp(-αh) << 1, we obtain from PhIWCM a simplified expression with further simplifications

$$PhIWCM \approx \eta \frac{h - \frac{1}{\alpha}}{\eta + m(1-\eta)} \approx \begin{cases} \eta\left(h - \frac{1}{\alpha}\right) \\ \kappa \eta h \end{cases} \left(\frac{2\pi}{\alpha HoA} \ll 1,\ e^{-\alpha h} \ll 1\right) \tag{3}$$

From (3) we see that the phase height is increasing linearly with height if the attenuation in the vegetation layer is increasing (e.g. the penetration depth is decreasing) or if $m = \sigma_{gr}^0 / \sigma_{veg}^0$ is decreasing. If m=1 and h>>1/α (e.g. h or α large, the latter as assumed in TLM [46]) we obtain Ph ≈ ηh, otherwise Ph is slightly less than ηh. ηh represents the mean canopy height, denoted IWCM MCH.

To estimate the meteorological influence, we can vary PhIWCM using Monte Carlo simulations over a range of α and m based on knowledge. With experience from Krycklan and Remningstorp we will assume α (the two-way attenuation) varies as uniformly distributed random numbers between 0.1 Np/m and 0.5 Np/m, corresponding to 0.4 dB/m and 2.2 dB/m and m between 0.4 and 2.5, see Fig. 2. Since an increase in α and a decrease of m has similar effect the earlier obtained values may have a certain coupling, cf. Fig. 2b with data from [47] [48].

The Monte Carlo simulations illustrate the possible variability of phase height. An expression, Phmean(HoA, n) is marked by solid black line in Fig. 2 representing an estimate without knowledge of the actual values of α and m.

$$Phmean(HoA, h, n) = PhIWCM(\alpha = 0.17, m = 1, HoA, h, n) \tag{4}$$

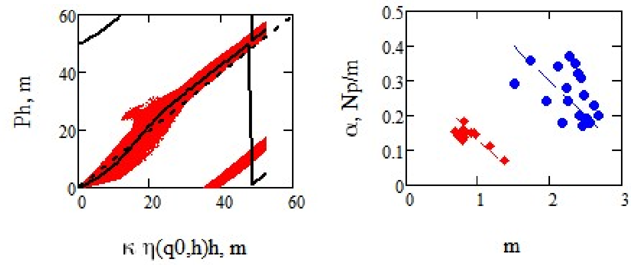

a b

Fig. 2. a) 10^5 Monte Carlo simulations of IWCM phase height with HoA 40, and 60 m (red dots) and the black solid line representing a mean phase height with the Phmean(HoA,h,n) with HoA as a mean of the those used for the simulation (40 m and 60m with different branches), and κ=0.90. b) Data for α and m for Krycklan (red) and Remningstorp (blue).

From Fig. 2 we see that Phmean is in close agreement with η(q0,h)·h and κ=0.9 for higher phase heights relevant for tropical forests. For lower phase heights a better expression is κ=0.8, an expression which is used for hemi-boreal and boreal test sites neglecting the influence of HoA. We see a higher uncertainty for heights below 30 m.

HoA has an influence which can be estimated as the mean HoA of the TanDEM-X acquisitions used for the DEM (see further below), h is the unknown forest height corresponding to H95 or Lorey's height (basal area weighted height) according to investigations in Krycklan e.g. [48] and Remningstorp e.g. [49] [45], and n is given by the branch of solutions used, i.e. resulting in an expression with only height as unknown.

Only the main branch of Phmean in the simulations is of interest, and we see that there is a phase change at Ph=50 (mean HoA) for Phmean while the simulation has a phase change at 40 m (and 60 m not shown). We see a larger variation around Phmean for lower phase heights, typical for boreal sites) and a smaller variation for higher phase heights, typical for tropical sites, which means that the height estimations of boreal sites using Phmean, due to lack of information on α and m, are expected to have lower accuracy than tropical sites.

V. Nomenclature

The datasets used in this study are the same as in [1]. High-resolution DTMs derived from airborne lidar data were available for all test sites at resolutions between 0.5 m and 2 m, and were averaged to 100 m resolution to match the expected BIOMASS DTM product. These DTMs represent elevations based on the last lidar return, although processing methodologies differ between sites. Top-of-canopy height (H100) and mean canopy height (MCH) were computed at 50 m spatial resolution from CHMs (Canopy Height Models) as the maximum and average height values, respectively, within each 50 m × 50 m grid cell.

200 sampling points (0.25 ha) were acquired from each of the sites [1]. These were used to determine phCOP, i.e. Copernicus 30 m – DTM difference, and relating to the corresponding

This article has been accepted for publication in IEEE Journal of Selected Topics in Applied Earth Observations and Remote Sensing. This is the author's version which has not been fu
content may change prior to final publication. Citation information: DOI 10.1109/JSTARS.2026.3722731

AGB, MCH and H100 (top-of-canopy height).

Nomenclature used in this paper

Symbol	Definition
phCOP	Copernicus DEM – DTM difference
$phCOP_{mean}$	Site mean of phCOP
Phmean	IWCM mean expression for phCOP
h_{est}	Estimated canopy height at pixel level, assumed to represent H95
h_{mean}	Site mean of h_{est}
h_{max}	Site maximum of h_{est}
AGB_{est}	Estimated AGB at pixel level
AGB_{mean}	Site mean of estimated AGB
RMSEr	Relative root mean square error
r^2	Coefficient of determination, Pearson's correlation coefficient squared
q0	Relating forest height to canopy density [3]

VI. Deriving Forest Properties

In [32] the mean phase height relationship Phmean(h) ≈ 0.8η(q0,h)h was applied to the observations from the semi-boreal Krycklan and the boreal Remningstorp sites. Here we apply the same formulation, but use forest-representative q0 values from [2] for all sites rather than locally estimated values. For tropical sites, we additionally take HoA into account, or alternatively apply 0.9η(q0,h)h, cf. Fig. 2. An expression for the Copernicus phase height consisting of e.g. N TanDEM-X acquisitions would be $Phmean(h) = \frac{1}{N}[\sum_n Phmean(HoA_n, h)]$, but the simpler *Phmean(HoAm,h)* with $HoAm = \frac{1}{N}\sum_n HoA_n$, provides equivalent results over the expected range of HoA variability and is applied here.

A. Forest height estimation

The forest height, the canopy height, h_{est}, is estimated from the mean phase-height and assumed to correspond to H95 when referred to phCOP, see e.g. [32]

$$root[Phmean(HoA, h) - phCOP] \qquad (5)$$

In order to take into account the first branch height interval we use *Phmean(HoA,h)* = *Phmean(HoA,h,0)* if *Phmean(HoA,h,0)* > 0 and otherwise *Phmean(HoA,h,1)*. H95 is not available in this analysis for comparison of h_{est}, and there is no simple relation between h_{est} and H100 as illustrated in Fig. 3 from Krycklan and Lopé, but we see that h_{est} is generally < H100, as expected. However, there is a large spread.

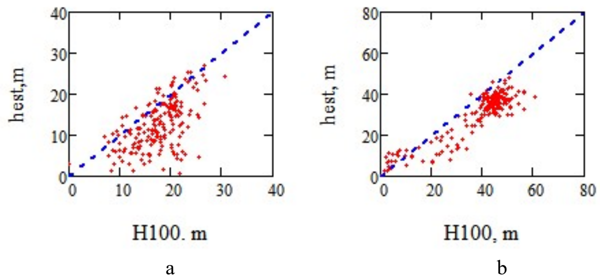

Fig. 3 Illustrating h_{est} versus H100 for a) Krycklan and b) Lopé

Instead of comparing h_{est} to H95, we can compare the IWCM MCH, i.e. $\eta(q0,h_{est})h_{est}$, with Lidar MCH, although principally different. It was shown by [1] that experimentally phCOP is close to Lidar MCH, (denoted only MCH in the following) which is the case for all sites. However, if we compare IWCM MCH and MCH we expect different relations for boreal and tropical forest heights, since phCOP is approximately described by 0.8η(q0,h)h and 0.9η(q0,h)h, respectively, cf. Fig. 2, related to the sensitivity to e.g. HoA as well as forest properties. In other words, we expect a difference in comparison of IWCM MCH and MCH for boreal and tropical forests when comparing RMSEr, r^2 and bias for the quantities, cf. Table 1, and we expect higher agreement for tropical sites.

TABLE 1 IWCM MEAN CANOPY HEIGHT, $\eta(Q0,H_{EST})H_{EST}$, VERSUS LIDAR MCH.

Site	r^2	RMSEr, %	Bias, m
Krycklan	0.65	54.0	0.78
Remningstorp	0.69	37.9	0.7
Lopé	0.91	17.2	1.84
Mabounie	0.72	13.1	-1.9
Mondah	0.95	16.5	0.27
Rabi	0.72	11.8	0.51
Nouragues	0.80	12.8	-1.25
Paracou	0.67	11.8	2.48

Krycklan and Remningstorp are managed areas and the 3–4-year difference between field data and Copernicus DEM means that relatively many changes have been made, including clear-cuts, resulting in a spread of the observations in Fig. 4 a) and b).

In [50] it was found that the mean canopy height was the most important predictor variable for biomass estimation from lidar across forest types from different continents including temperate and tropical forests. We can then expect that phCOP is not only close to MCH but also close to AGB, which also was shown in [1] by correlation, and in [32] for the boreal sites, and will be further investigated below.

This article has been accepted for publication in IEEE Journal of Selected Topics in Applied Earth Observations and Remote Sensing. This is the author's version which has not been fu
content may change prior to final publication. Citation information: DOI 10.1109/JSTARS.2026.3722731

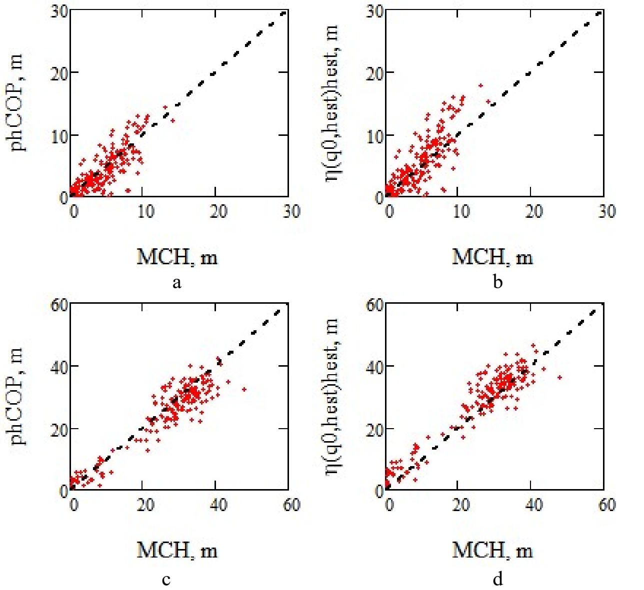

Fig. 4. Illustrating phCOP and IWCM mean canopy height $\eta(q0,h_{est})h_{est}$ versus MCH a), and b) Krycklan and c) and d) Lopé (note different scales).

B. AGB models

For AGB estimation we will use training pixels from the studied site. Approximately 5% of the 0.25 ha pixels will be used, in order to choose a small number for training. Three expressions for AGB will be studied:

$$AGB_a = a h_{est}^{b} \tag{6a}$$
$$AGB_b = \kappa_0\, phCOP \tag{6b}$$
$$AGB_c = \kappa_b \cdot \eta(q0, h_{est}) \cdot h_{est} \tag{6c}$$

where a, b, κ_0, and κ_b, are determined from the training pixels and h_{est} is determined from phCOP as given in (5).

The expression $AGBa = a \cdot h_{est}^{b}$ is commonly used for a relation between AGB and height, e.g. [4] [19]. Investigations indicate that the main error of a height-biomass allometry is missing information of forest density or basal area, see e.g. [51], this is why the other two expressions are applied. (6b) was introduced by [52] for TanDEM phase height rather than phCOP. More recently [1] identified different values of κ_0 for boreal, temperate and tropical sites and also a mean value for all sites using Copernicus DEM – DTM difference, i.e. phCOP. AGB is intuitively related to density times height, (6c), cf. [53] [45]. With the close relation between phCOP and IWCM MCH, $\eta(q_0,h_{est})h_{est}$, we only expect minor differences, between (6b) and (6c), related to the derivations and the site properties.

To determine a and b we introduce h(a,b,AGB) expressed from (6a) and obtain Phmean(HoA, a, b, AGB). a and b are obtained from

$$min[\sum(Phmean(HoA, a, b, AGB) - phCOP)^2] \tag{7}$$

where the summation takes place over the training pixels with known AGB-values.

For the other two expressions, κ_0 and κ_b, are obtained by minimizing the difference between the left minus the right-hand side expression, squared, and summed over the training pixels, similar to (7). Note that in [1] all pixels are used for comparing the left and right side of (6b) while here 5% training pixels are used for estimating e.g. κ_0, leading to some differences.

The obtained parameters, a, b, κ_0, and κ_b, are valid for the specific forest type for which they are derived. We have shown that that the phase height for tropical forest can be approximated by $0.9\eta(q_0,h_{est})h_{est}$ and with that relation we expect from (6b) and (6c) that $\kappa_b/\kappa_0 \approx 0.9$ for the tropical sites, and we obtain 0.83 ± 0.03 when we take HoA into account, illustrating the agreement between the assumed expressions and the observed phCOP and AGB values.

Below we will present the results of the calculations and finally associate the observed values of κ_0 and κ_b for the different sites characterized by their mean height and q0-values.

Since AGB is our primary aim it should be noted that the reference values for the tropical sites are from the AfriSAR and TropiSAR campaigns [6], where initially AGB was estimated at the tree level from the measured DBH, the tree height information, the wood density information together with a biomass allometric equation. In the end median canopy height, H50, was considered the best predictor of AGB in "all-sites" models and the RMSEr were 23.6% at 0.25-ha resolutions [6].

VII. RESULTS

A. Forest height and AGB

The derived results from the different sites are illustrated by three figures from each site, see Fig. 5. The first illustrates phCOP versus AGB for the training pixels (blue), and for the test pixels (red) and also Phmean as function of AGB (dashed blue line) from the training pixels, the second figure illustrates h_{est} versus AGB and the derived relations AGB(h), see below, the final figure illustrates the two AGB expressions κ_0 phCOP (red), $\kappa_b \cdot \eta(q0,h_{est}) \cdot h_{est}$ (blue) and the diagonal (blue dashed) for the training pixels versus AGB. The first two sets of figures are from Krycklan and Remningstorp, the following four from Gabon and the final two from French Guinea.

From the leftmost figures we conclude that the relation between phCOP and AGB is almost linear for most sites. In the middle figure we derived ah^b from the training pixels for phCOP (blue dashed line) and from $\kappa_b\eta(q0,h_{est})h_{est}$ (black dashed line) where κ_b is determined from the training pixels while h_{est} is from all pixels). In the first case two unknowns are determined from the few training pixels, while in the second case it is one unknown, which is the better case when characterizing h_{est}.

Krycklan and Remningstorp are managed areas and the time difference between DEM data and in situ data from Krycklan 2008 and Remningstorp 2010 means that some of the points changed in the meantime and should be excluded. For this reason, phCOP and MCH have been compared and phCOP-points larger than 1.5 MCH and less than $0.6\eta(q_0,MCH)MCH$ have been excluded. This effects mainly the two boreal sites, but we still see a relatively large spread in Fig. 5 for those sites. Part of this is related to the high resolution. In [32] Krycklan and Remningstorp were investigated with the same technique but using stands larger than 1 ha in Remningstorp and 2.4 ha in Krycklan, with less scattering. Finally, it should be noted that Mondah is different from the other tropical sites with a more continuous set of forest heights.

The total number of points, N_{tot}, considered, and the number of training points N_{tr}, are listed in Table 2 together with h_{max}, h_{mean} and AGB_{mean}. In Table 3 the $AGB=ah^b$ related parameters for the black dashed line in Fig. 5 are listed, and in Table 4 the accuracy of estimated AGB relative lidar values.

If in situ values for forest height are available, we can with the derived a- and b-values, estimate α_{eff} and m_{eff} by minimizing

$$min\{\sum(PhIWCM(\alpha,m,HoAm,h(a,b,AGB)) - phCOP)^2\} \tag{8}$$

over the training sites. The resulting values are listed in Table 5.

N_{tot}, total number of observation points, N_{tr} number of training points, h_{max} max estimated height for the site, h_{mean}, mean estimated height for the site, AGB_{mean}, mean estimated AGB for the site, q0 for Krycklan and Remningstorp changed relative [32] where local values were used while here the forest type is decisive and available world-wide in [2].

From Table 4 we see that the best AGB accuracy is obtained for the two expressions $\kappa_0$phCOP and $\kappa_b\eta(q0,h_{est})h_{est}$ with mean values for the tropical sites of the latter expression of 17.6% while for the boreal sites we have 43.8%. For the tropical sites r^2 for the AGB expression is 0.73 indicating the strength of (4) as the starting point for Ph_{mean}.

Finally, the two-parameter AGB_a expression (black dashed line in Fig. 5) is illustrated in Fig. 6 illustrating some difference between the BioSAR, AfroSAR and TropoSAR sites.

B. Mean forest height and mean AGB.

That AGB is dependent on forest height is well known and also illustrated by (6), see also [54] [55]. The importance of mean forest height is stressed in [50]. Based on e.g. airborne TomoSAR at P-band the forest layer at about 30 m has been known to relate with high accuracy to AGB [24] [25] [56]. In Fig. 7 we illustrate the mean AGB versus the mean height for the investigated sites and we see that there is a relation and that most tropical sites with mean AGB in the range 300 – 400 Mg/ha (all sites but Mondah) have their mean estimated AGB associated with the mean height about 30 m. We also see that the accuracy of the mean estimated AGB is increasing with mean height and 11% - 17% for the tropical sites with a mean height about 30 m. This can be compared with the similar results using airborne P-band TomoSAR in TropSAR with a resolution of 1.5 ha [24] [25]. The two remote sensing techniques can then complement each other since they are sensitive to different forest properties.

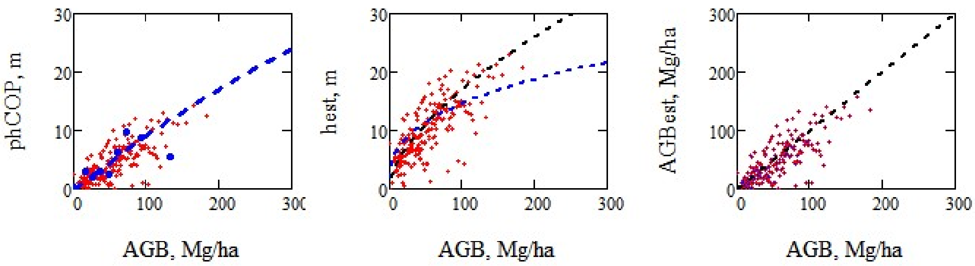

a. Krycklan

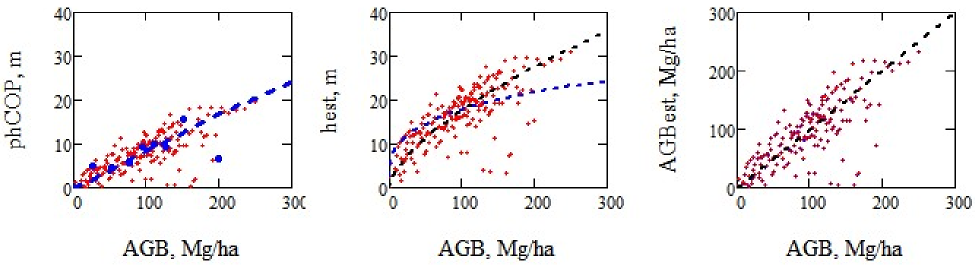

b. Remnintstorp

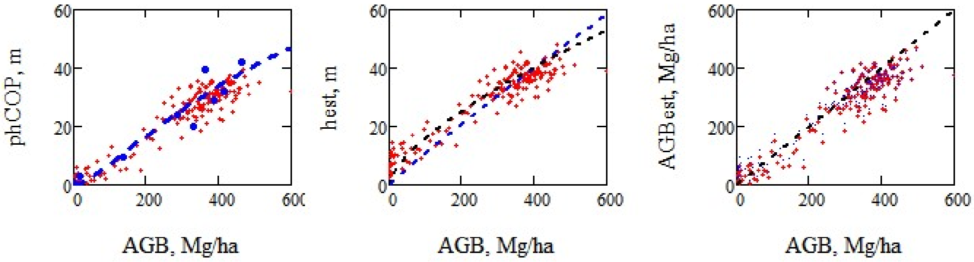

c. Lopé

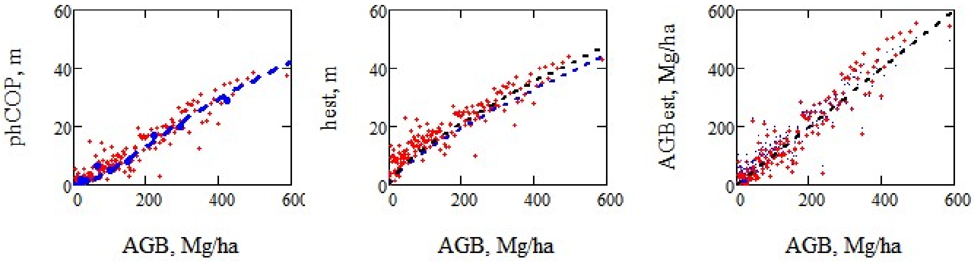

d. Mondah

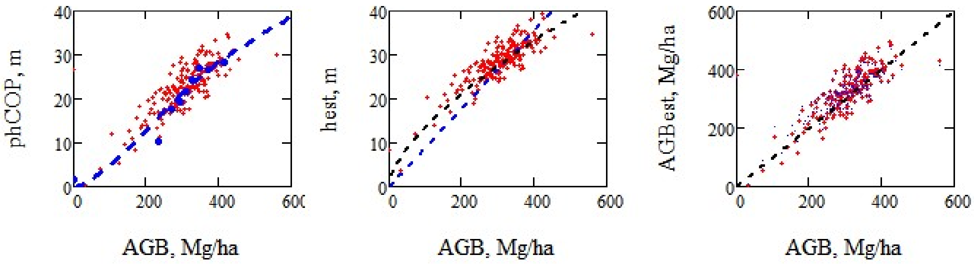

e. Mabounie

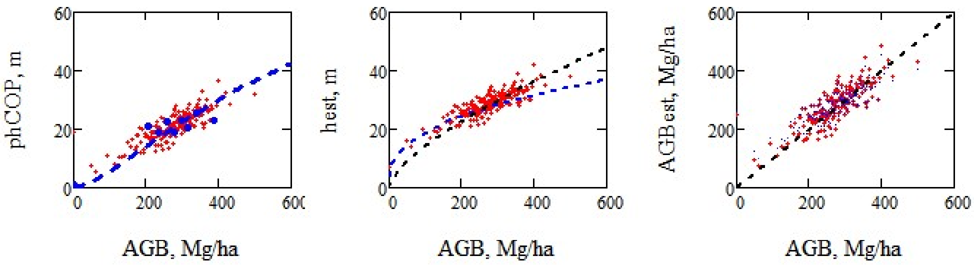

f. Rabi

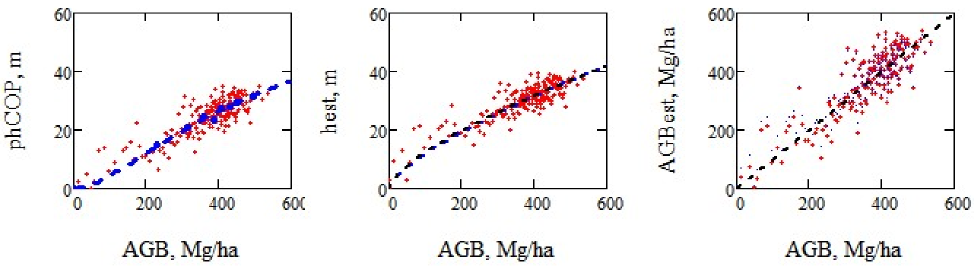

g. Nouragues

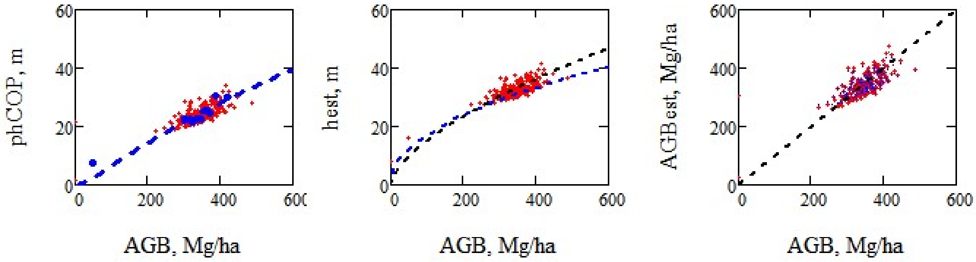

h. Paracou

Fig. 5. Results for studied sites. The leftmost figure shows phCOP versus AGB, the middle figure h_{est} versus AGB, and the rightmost figure the estimated AGB versus the reference AGB. The blue and black dashed lines in the figures of h_{est} versus AGB represents the ah^b relation derived in two different manners, se text. The red and blue points in the figures on AGB_{est} versus AGB show the results of (6b) and (6c) respectively. The derived theoretical relation or reference line is marked by dotted blue lines. Note the different scales.

TABLE 2. BASIC INFORMATION ABOUT THE INVESTIGATED SITES AND DERIVED RESULTS.

Site	N_{tot}	N_{tr}	q0	h_{max}, m	h_{mean}, m	AGB_{mean}, Mg/ha
Krycklan	189	9	0.04	27	12.4	62.5
Remningstorp	186	9	0.05	34.2	16	134
Lopé	186	9	0.07	48.1	28.7	279.7
Mabounie	191	9	0.07	39.3	28.5	328.2
Mondah	182	9	0.07	44	17.5	166.4
Rabi	191	9	0.07	41.8	28.6	294.9
Nouragues	190	9	0.08	39.8	29.1	367.2
Paracou	191	9	0.08	40.8	32	341.2

TABLE 3. COEFFICIENTS IN AGB-EXPRESSIONS. A AND B PARAMETERS IN $AGB_C(H)=AH^B$ (BLACK DASHED LINE IN FIG. 5), $\kappa 0$ IN $AGB_B=\kappa 0$ PHCOP, κB IN $AGB_C=\kappa_B\eta(Q0,H_{EST})H_{EST}$,

Site	a	b	κ_0	κ_b
Krycklan	0.58	1.71	10.92	8.82
Remningstorp	1.08	1.57	11.88	9.57
Lopé	1.6	1.49	11.62	10.3
Mabounie	1.86	1.53	14.22	13.07
Mondah	2.65	1.4	14.4	12.03
Rabi	1.88	1.49	13.38	11.45
Nouragues	2.27	1.5	15.35	13.81
Paracou	1.33	1.6	14.07	11.6

TABLE 4. AGB ESTIMATION PROPERTIES USING THREE AGB MEASURES: PEARSON R^2, RMSER, AND BIAS FOR ASSOCIATED EXPRESSION, IN THREE AGB-EXPRESSIONS, (6 A,B,C).

Site	r^2_a	$RMSEr_a$ %	$Bias_a$ m	r^2_b	$RMSEr_b$ %	$Bias_b$ m	r^2_c	$RMSEr_c$ %	$Bias_c$ m
Krycklan	0.57	93.77	5.74	0.57	49.43	-7.6	0.57	49.53	-7.73
Remningstorp	0.61	126.43	36.19	0.61	38.03	-2.68	0.61	38.11	-2.78
Lopé	0.9	17.3	-6.26	0.9	18.63	-23.6	0.9	17.78	-15.35
Mabounie	0.61	16.62	22.69	0.61	17.48	19.37	0.61	16.61	20.87
Mondah	0.89	31.63	12.78	0.89	30.76	6.8	0.89	30.37	17.01
Rabi	0.62	32.85	19.8	0.67	15.19	7.85	0.67	15.01	8.9
Nouragues	0.75	17.27	5.34	0.77	15.66	4.42	0.77	14.98	8.23
Paracou	0.44	15.51	-3.28	0.51	11.1	-2.33	0.51	10.83	-1.78

TABLE 5. A_{EFF} AND M_{EFF} WITH KNOWN MCH

Site	HoA_m m	α_{eff} Np/m	m_{eff}
Krycklan	68.7	0.19	0.7
Remningstorp	39.6	0.15	0.7
Lopé	100.5	0.21	0.7
Mabounie	54.1	0.14	0.34
Mondah	77.7	0.26	0.7
Rabi	77.9	0.2	0.7
Nouragues	55.7	0.17	0.7
Paracou	439.8	0.26	0.7

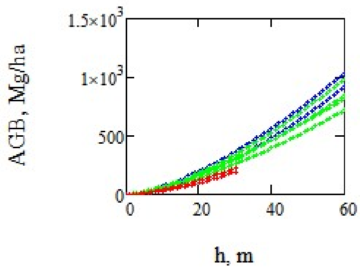

Fig. 6. Illustrating derived $AGBc= ah_{est}^b$ for BioSAR sites (red), AfroSAR sites (green), and for TropoSAR sites (blue)

The relative results in the form of RMSEr-values are best for dense tropical sites of which Mondah differ due to a lower mean height and mean AGB. Tree height for a given diameter is

This article has been accepted for publication in IEEE Journal of Selected Topics in Applied Earth Observations and Remote Sensing. This is the author's version which has not been fu
content may change prior to final publication. Citation information: DOI 10.1109/JSTARS.2026.3722731

consistently lower than at other sites and a site-specific height-DBH relationship had to be developed. The consequent behavior with decreasing AGB and increasing RMSEr values for low mean height indicates that the method using Copernicus DEM is best used for tropical sites. This can be related to the accuracy of the Copernicus DEM, see below, and the higher sensitivity to the attenuation and the ground/crown scattering for lower heights, see Fig. 2, and the associated uncertainty in the expression for the mean phase height in the used method. For the boreal sites the method using TanDEM-X phase-height in combination with coherence and backscatter has given RMSEr- values better than 20% [45] [47] [48] [57] and was also demonstrated in [32] using the present method applied on the mean of TanDEM-X phase heights but using stands >1 ha.

The RMSEr related to the derived ah^b expression for AGB (black dashed in Fig.5) is not varying as consistently as the other two expressions for AGB, which probably is due to the need to estimate two parameters, a and b.

Finally, we illustrate in Fig. 8 the total AGB_{mean} error varying between 47.7±9.8 Mg/ha for the sites (given with one standard deviation). Since we have a direct relation between AGB_{mean} and mean phase height we can also associate an approximative error to the mean phase height which (in the case of an accurate DTM) can be attributed the Copernicus DEM for which we obtain a mean error with a standard deviation of less than 3.6±0.6 m. A not insignificant part is due to the small number of training pixels. A relative constant error of the Copernicus

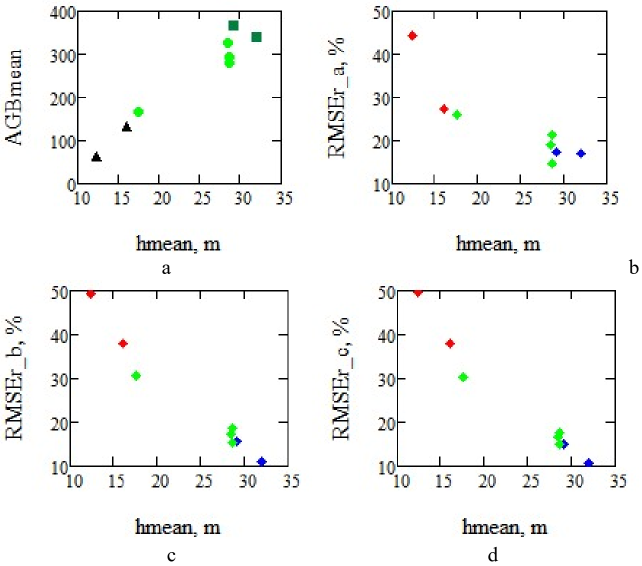

Fig. 7 Illustrating mean AGB in Mg/ha and RMSEr versus mean height for the investigated sites, a) mean AGB for the sites, b) – d) RMSEr for different methods to estimate mean AGB. Red marks BioSAR sites, green AfriSAR sites, and blue TropiSAR sites.

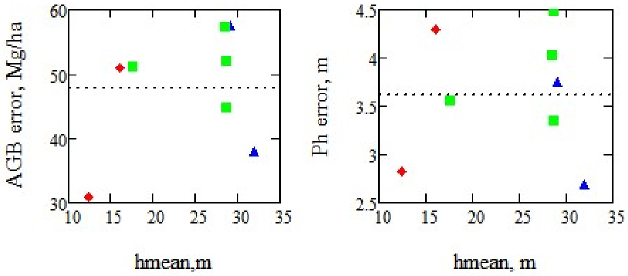

Fig. 8. a) AGB error in Mg/ha versus h_{mean} in m and b) error in mean phase height for the different sites. Red marks: BioSAR sites, green: AfriSAR sites, and blue: TropiSAR sites, mean error dotted,

DEM demonstrates why the present method gives higher AGB errors for forests with a lower forest height.

C. *AGB methods without training data*

So far, we have studied expressions for AGB using 5% of the observations as training data, but an important question is to what extent we can avoid training data since training pixels for AGB are not available under most conditions. For that purpose, we study the derived parameters κ_0 and κ_b relative a parameter which can be derived separately, such as q0 which is related to the type of forest, or some height measure which can be determined from phCOP, such as h_{mean}. This is not possible for the a and b-coefficient in (6a) although there is a certain relation between a and b and the curves as seen in Fig. 6. However, κ_0 and κ_b exhibit an almost linear relation to q_0, see Fig. 9. r^2 for κ_0 versus q_0 is 0.66 and r^2 for κ_b is 0.68.

The linear interpolation between κ_0 and κ_b versus q0 in Fig. 9 is very close to the more complex interpolation line, and we obtain alternative expressions for κ_0 (relating Copernicus DEM-DTM difference to AGB) and κ_b (relating $\eta(q0,h_{est})h_{est}$ to AGB).

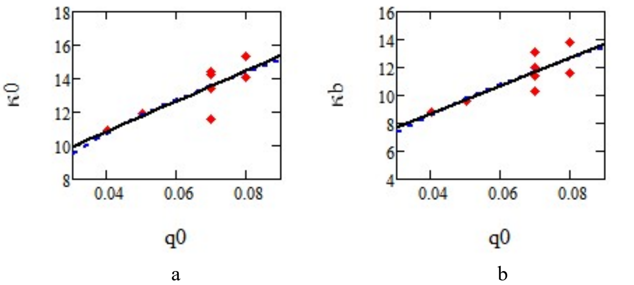

Fig. 9. Relation between a) κ_0 and q0 and b) κ_b and q0 (solid line: linear interpolation, dotted line fitted relations $41.6q0^{0.420}$ and $56.5q0^{0.837}$ resp.)

$$\kappa alt_0 = 90.80q0 + 7.22 \qquad \text{stdev } 0.99 \qquad (9a)$$
$$\kappa alt_b = 90.50q0 + 4.74 \qquad \text{stdev } 1.03 \qquad (9b)$$

The accuracy of the AGB estimation using the q0-related coefficients (9) is presented in Table 6.

Using the alternative κ-parameters (9) the RMSEr accuracy using κalt_0 is decreased with 2.8±3.4 percent units and using κalt_b with -0.2±1.2 percent units compared to the training case. An important point with (9) is the clear dependence of q0 on the relation between AGB and the observables.

A second alternative to derive AGB without training is to study the relation between AGB_{mean} and h_{mean} as illustrated in Fig. 7. Since $\eta(q0,h_{est})$ has its largest influence for small h_{est}, see Fig. 1, we also have a close relation between h_{est}, and AGB (see Fig. 10b for Mondah). If we determine AGB_{mean} and h_{mean} (marked in Fig. 10 by black dots) we find a close to linear relation between the values for all sites as illustrated in Fig.11.

$$AGB1_{mean} = 14.40h_{mean}-100.14 \quad (10a)$$
$$ABG2_{mean}=13.6\, phCOP_{mean} +15.12 \quad (10b)$$
$$AGB3_{mean} = 11.65\,\eta(q0,h_{mean})h_{mean} +19.61 \quad (10c)$$

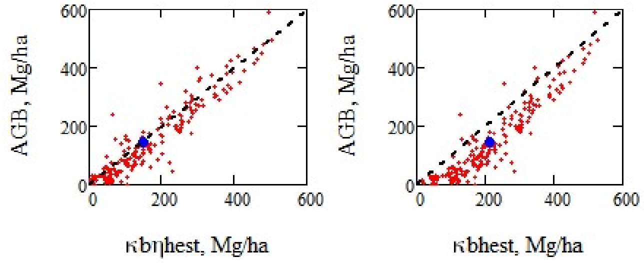

a b

Fig. 10. Illustrating a) $\kappa_b\eta(q0,h_{est})h_{est}$ versus AGB and b) $\kappa_b h_{est}$ versus AGB for Mondah. The points corresponding to h_{mean} and AGB_{mean} are marked by a black circle.

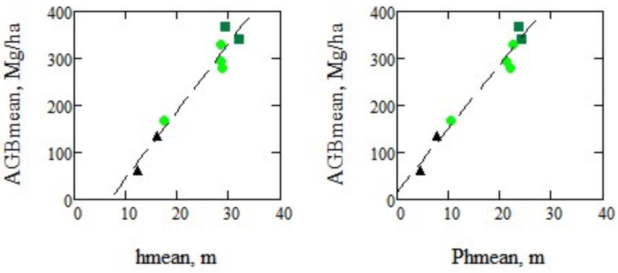

a b

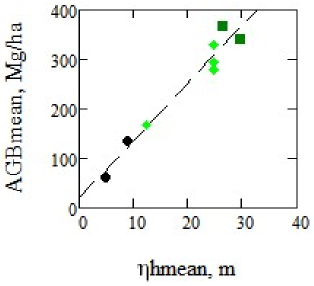

c

Fig. 11. Illustrating a) AGB_{mean} versus h_{mean}, b) AGB_{mean} versus Ph_{mean} and c) AGB_{mean} versus $\eta(q0,h_{mean})h_{mean}$, for all sites; from BioSAR black points, from AfriSAR light green points and from TropiSAR dark green points.

Using the fitted linear regression (9) we obtain estimates of how AGB_{mean} varies with h_{mean}, $phCOP_{mean}$, and $\eta(q0,h_{mean})h_{mean}$ for the investigated sites. From (9b) and (9c) we have expressions for AGB_{mean} and can now determine κ_0 and κ_b by minimizing the following expression

$$\kappa_0 = \min[AGB3_{mean} - \kappa_0 mean(phCOP_{st})] \quad (11a)$$
$$\kappa_b = \min[AGB1_{mean} - \kappa_b mean(\eta(q0,h_{est})h_{est}] \quad (11b)$$

The obtained coefficients are also assumed relevant for each pixel value.

(9b), illustrated in Fig. 11b, differs from the mean AGB for the site by -9.98 Mg/ha with a standard deviation of 19.31 Mg/ha for all sites and by -6.71 Mg/ha as a mean with a standard deviation of 20.20 Mg/ha for the tropical sites. (9c), illustrated in Fig. 11c, differs from the mean AGB for the site by zero Mg/ha with a standard deviation of 23.88 Mg/ha for all sites and by 0.23 Mg/ha as a mean with a standard deviation of 27.10 Mg/ha for the tropical sites. The coefficient of determination, r^2, is 0.94 for AGB_{mean} versus h_{mean}, 0.97 for AGB_{mean} versus $phCOP_{mean}$ and 0.98 for AGB_{mean} versus $\eta(q0,h_{mean})h_{mean}$.

D. Test of AGB estimation without training

Three temperate forest sites: Kermeter in Germany, Białowieza in Poland, and Warra in Tasmania, Australia considered in [1] were not included above since the AGB reference data were deemed less reliable than those obtained from ESA campaigns. Nevertheless, since these sites were excluded from the earlier analysis, they can be analyzed using the suggested AGB estimation method that does not require training data.

According to [1] airborne LiDAR data were collected between 2011 and 2018 for these three sites by different research teams using various systems and methodologies. In Białowieża, five forest strata were defined, and for each, AGB was estimated from the median canopy height using 629 plots (0.05 ha each) distributed across the entire site. In Kermeter, an AGB map was generated using a machine learning approach supported by local in situ measurements and terrestrial laser scanning data. In Warra, AGB was estimated from the canopy height model (CHM).

To estimate biomass, a functional relationship between the observable parameters and AGB is required. In previous analyses, three reference expressions (9a), (9b), and (9c) were defined for AGB_{mean} in terms of the observables q0 and phCOP,

TABLE 6 ACCURACY OF AGB ESTIMATION WITHOUT TRAINING PIXELS BUT BY MEANS OF Q0 FROM [3] AND (9).

Site	κalt_0	κalt_b	Results with κalt_0			Results with κalt_b		
			RMSEr %	r^2	Bias, Mg/ha	RMSEr %	r^2	Bias, Mg/ha
Krycklan	10.4	8.14	45.65	0.57	-9.96	51.11	0.57	-11.48
Remningstorp	11.36	9.22	27.58	0.61	-6.8	37.86	0.61	-6.3
Lopé	13.3	11.38	18.52	0.9	14.4	16.94	0.9	12.89
Mabounie	13.3	11.38	14.6	0.61	-1.81	16.41	0.61	-21.37
Mondah	13.3	11.38	26.21	0.89	-5.47	28.68	0.89	7.75
Rabi	13.3	11.38	14.05	0.67	6.17	14.89	0.67	7.15
Nouragues	14.27	12.46	15.89	0.77	-21.51	16.62	0.77	-27.92

This article has been accepted for publication in IEEE Journal of Selected Topics in Applied Earth Observations and Remote Sensing. This is the author's version which has not been fully edited and
content may change prior to final publication. Citation information: DOI 10.1109/JSTARS.2026.3722731

Paracou	14.27	12.46	11.24	0.51	2.27	12.85	0.51	23.59

and h_{est} (derived from phCOP). These expressions enable the estimation of the mean reference AGB for each site according to the behavior established from the eight analyzed sites and their dependence on the parameter q0.

TABLE 7. VALUES AVAILABLE FOR AGB ESTIMATION

Site	q0, m^{-1}	HoAm, m	$phCOP_{mean}$, m	h_{mean}, m
Bialowieza	0.050	39.7	17.6	27.9
Kermeter	0.050	106.4	16.0	23.3
Warra	0.065	114.1	27.2	34.5

(5) is used to derive h_{est} from phCOP and (9) and (10) are used to derive the corresponding AGB. The resulting AGB estimates obtained without training data are shown in Fig. 12 (d) – (f), plotted against the corresponding reference AGB values for the three investigated sites, and for comparison the corresponding figures for AGB using 5% training stands in (a) – (c). A quantitative summary of these results is provided in Tables 8 and 9. The relative root mean square error (RMSEr) values are found to be somewhat higher (on average two percent units) to those reported by [1], who derived them by estimating the linear slope between all the observations of phCOP and AGB - the optimal relation for the studied dataset.

The result based on (9a) with phCOP proportional to AGB is the better alternative and comparing with the last column in Table 9 approximately the same as when training is used. The RMSEr values of the three sites are correlated with the mean canopy height, r^2=0.93 (Fig. 7), and RMSEr is approximately ten percentage points higher than for the original sites analyzed using training data as illustrated in Fig. 13. With the close agreement between RMSEr with and without training, Table 9, the higher RMSEr values are primarily caused by less accurate field-based reference AGB measurements, possibly in combination with more complex forest structures.

The relation between RMSEr and h_{mean} in Fig. 13 is

$$RMSEr(h_{mean}) = 1470 h_{mean}{}^{-1.342} \qquad (12)$$

TABLE 8. ESTIMATED VALUES FOR SITES WITHOUT THE USE OF TRAINING PIXELS.

Site	κalt_0	Max h_{est}, m	Mean h_{est}, m	Max AGB_{est} Mg/ha	Mean AGB_{est} Mg/ha
Bialowieza	11.7	40.6	27.9	815.5	208
Kermeter	11.7	37.3	27.3	449.6	218.2
Warra	13.6	55.9	34.5	649.8	339.4

TABLE 9. RMSER OBTAINED WITHOUT TRAINING FOR THREE SITES USING (9) OF (10) COMPARED WITH RMSER USING TRAINING AND (6B).

Site	RMSEr, %	RMSEr, %	RMSEr, %	RMSEr, %	RMSEr, %	RMSEr, %
Equation	(9a)	(9b)	(10a)	(10b)	(10c)	(6b)
Bialowieza	26.4	28.8	46.5	30.5	33.0	26.7
Kermeter	28.3	32.8	39.1	27.4	28.7	28.6
Warra	19.9	16.2	18.6	22.2	19.1	18.7

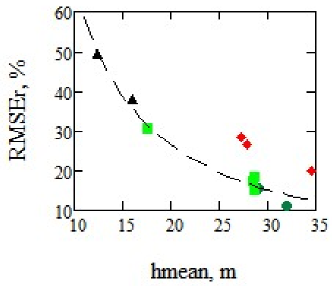

Fig. 13. RMSEr derived using AGB = κ_0· phCOP and 5% training pixel for the BioSAR, AfriSAR, and TropiSAR reference sites are shown in black, light green, and dark green, respectively. The three temperate sites with RMSEr derived without training pixels and with RMSEr derived using AGB = κalt_0· phCOP are shown in red.

Finally, we compare the results obtained in this paper by the method in [1]. i.e. AGB=k·copPh with k given for different forest types in Tables 11 and 12 The input data are the same in the two cases. Comparing the two tables we see that r^2 is better in Table 11, which is natural since those results are based on optimal correlation. However, RMSEr in Table 10 is better than or similar to those in Table 11, and bias is in equal number of cases best in each one of Tables 11 and 12 in spite of the long way between the starting point and the results in case of Table 10 with errors involved in the different steps, illustrating the strengths of the simple approach used in [1] as well as the model analysis in the present analysis.

TABLE 10 RESULTS DERIVED IN THIS PAPER, AGB=κALT_0·COPPH

Site	κalt_0	RMSEr %	Bias, Mg/ha	r^2
Krycklan	10.4	45.7	-9.96	0.57
Remningstorp	11.36	27.6	-6.8	0.61
Bialowieza	11.74	26.4	-9.76	0.47
Kermeter	11.74	28.3	-25.88	0.53
Warra	13.56	19.9	15.24	0.81
Lopé	13.30	18.5	14.4	0.9
Mabounie	13.30	14.6	-1.81	0.61
Mondah	13.30	26.2	-5.47	0.89
Rabi	13.30	14.1	6.17	0.67
Nouragues	14.27	15.9	-21.51	0.77
Paracou	14.27	11.2	2.27	0.51

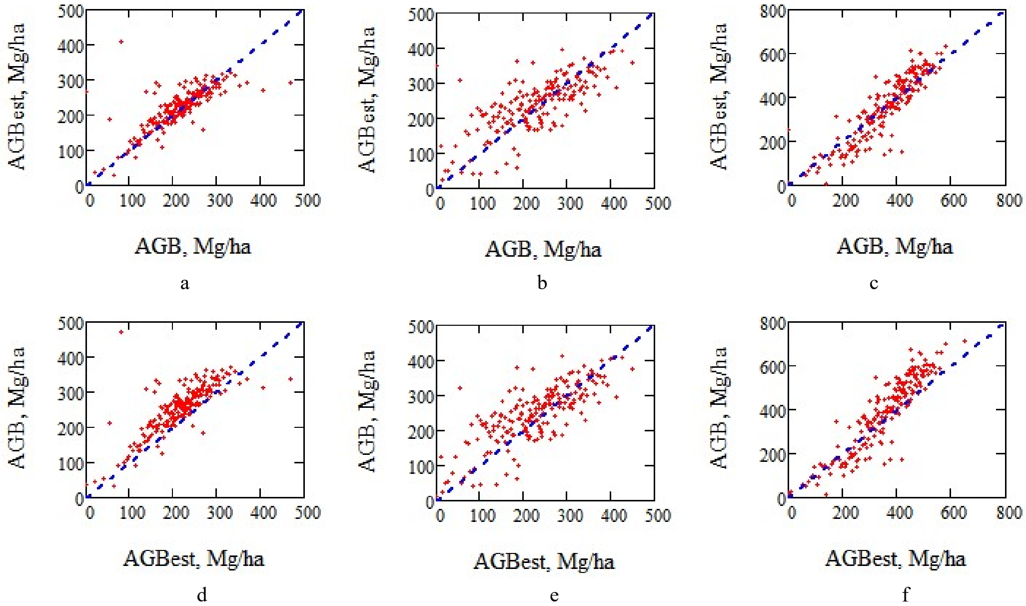

Fig. 12. Estimated AGB with (upper row) and without (lower row) training versus reference AGB for Bialowieza (a,d), Kermeter (b,e), and Warra (c,f) based on AGBest=$\kappa_0$phCOP and AGBest=κalt_0phCOP resp.

TABLE 11 Results derived with the model from [1], AGB=kSoja·copPh

Site	kSoja	RMSEr %	Bias, m	r^2
Krycklan	11.44	51.2	-5.34	0.58
Remningstorp	11.44	40.3	-6.58	0.63
Bialowieza	12.64	25.5	5.04	0.55
Kermeter	12.64	26.7	-12.86	0.61
Warra	12.64	17.8	-11.66	0.84
Lope	13.60	20.8	22.95	0.91
Mabounie	13.60	13.7	2.41	0.74
Mondah	13.60	30.5	-2.6	0.9
Rabi	13.60	14.6	11.53	0.72
Nouragues	13.60	22.8	-63.12	0.8
Paracou	13.60	14.5	-40.05	0.65

VIII. Discussion

Some points in the presentation will now be discussed:

The two-way attenuation coefficients and ground-to-canopy scattering ratios were based on data from Krycklan and Remningstorp. With MCH is known, values of α_{eff} and m_{eff} can be determined (Table V), and the κ_b/κ_0 ratio of 0.83, based on observed phCOP and AGB, are resulting in values that illustrate the relevance of the present analysis also for tropical forests.

Local variability of q0 is assumed to be of limited importance because $\eta(q_0,h)h$ generally varies only weakly (Fig. 1). A variation of ±10% in q0 has a negligible influence on the results, except for AGB estimation in Krycklan and Remningstorp, where the two-parameter expression ah^b shows a certain sensitivity. This appears to be associated with the reduced accuracy resulting from the estimation of two unknown parameters in the AGB retrieval (Fig. 5 and Table IV). Consequently, (6a) is not considered suitable for AGB retrieval in boreal sites.

For Mondah we obtained RMSEr=31%, which is high for a tropical forest. Forest structure can be of importance but a h_{mean} of 17.5 m, compared with more than 28 m for the other tropical sites, is assumed of primary importance related to the DEM height error. Fig. 13 shows that Mondah follows the general trend observed for the proposed method.

Differences in forest structure, also contribute to the observed variations and are assumed to be important for the temperate sites combined with uncertainties in field data. Since κ_0 was also estimated using training data, its difference relative to κalt_0, obtained without training, could be evaluated. The differences were found to be +0.83, +0.61, and −0.67 Mg/m^3 for Bialowieza, Kermeter, and Warra, respectively, all within the standard deviation of κalt_0 (0.99 Mg/m^3). The accuracy of the reference data therefore remains a possible limiting factor.

Finally, an important methodological aspect concerns the use of IWCM rather than the more commonly applied RVoG model. A key difference between the two approaches is that IWCM explicitly includes density as a parameter, requiring independent site information. In the present study, this requirement is addressed through q0. In contrast, RVoG assumes a homogeneous medium and employs an effective attenuation coefficient, which is more difficult to interpret physically. Biomass is in this paper characterized as being proportional to the product of height and density. The resulting parameters are found to follow a systematic ordering with respect to q0, suggesting that density remains an important variable even for tropical forests observed at X-band.

A limitation of the present method is that such a DEM can only be updated a limited number of times unless future satellite missions ensure continued availability, and a suitable DTM is not yet generally available.

An advantage of the present analysis is that the classification based on q0 is more detailed than the three broad classes considered in [1]. Furthermore, height as well as biomass can be estimated and h_{mean} can be used to assess the expected retrieval accuracy.

The main advantage is that the high-resolution, saturation-free method identified in [1], represents a complementary approach for biomass mapping.

IX. Conclusion

The goal of this paper is to investigate the proportionality between Copernicus DEM – DTM, denoted phCOP, and AGB, described by Soja et.al. in [1], now by means of physically related models instead of statistical correlation, using the same dataset. For six tropical and two boreal sites from three continents with ESA field campaigns, phCOP is interpreted through the semi-empirical IWCM. Forest height (judged to correspond to H95 or Lorey´s height) as well as the IWCM mean canopy height are derived from phCOP, with factors related to q0, a parameter derived from ICESat [2] and used as geolocator and a forest type parameter. AGB is first estimated by means of training using 5% of the observed points.

From the sites with ESA field campaigns a strong relationship, $r^2 = 0.97$, was identified between site means $phCOP_{mean}$ and AGB_{mean}, 0.98 for AGB_{mean} versus $\eta(q0,h_{mean})h_{mean}$, and 0.94 for AGB_{mean} versus h_{mean}, where h_{mean} is directly obtained from phCOP and q0 for the field site for which AGB is estimated. These relationships enable estimation of AGB at other sites without the need for local training.

If the Copernicus DEM uncertainty is assumed to be the principal error source, this error is estimated to less than 3.6 m for the studied sites. Accordingly, the relative RMSE is lowest for tropical forests, with RMSEr 11-18 % for the tropical sites with h_{mean} above 25 m.

Without training points the RMSEr for three additional temperate sites on two continents were roughly equal to the values obtained with training pixels but higher than expected from the reference sites, probably related to less accurate reference AGB values or more complex forest structures.

Overall, the present analysis demonstrates that a physically based interpretation of DEM height relative to a DTM provides a consistent explanation for the relationship between Copernicus DEM and AGB illustrated in [1]. The proposed framework requires only generally available high-resolution DEM and ICESat-derived information, making it applicable on a global scale once a suitable DTM is available and offers a complementary approach to satellite biomass retrieval.

Declaration of Competing Interest

The author declare that he has no competing financial interests or personal relationships that could have appeared to influence the work reported in this paper. No financial support has been obtained.

Acknowledgement

Maciej Soja and his co-authors in [1] are gratefully acknowledged for the data on phCOP, MCH, H100, and reference AGB used in this paper, and on which the analysis is based. Maciej Soja, Lars Ulander and a reviewer are also gratefully acknowledged for comments.

References

[1] M. J. Soja, M. Santoro, F. Banda, S. Tebaldini, M. Lisiewicz, K. Stereńczak, *et al.*, "Sub-hectare resolution forest biomass mapping from Copernicus DEM with low-dimensional models," *Science of Remote Sensing,* vol. 12, p. 100250, 2025.

[2] H. Kay, M. Santoro, O. Cartus, P. Bunting, and R. Lucas, "Exploring the Relationship between Forest Canopy Height and Canopy Density from Spaceborne LiDAR Observations," *Remote Sensing,* vol. 13, p. 4961, 2021.

[3] WMO, "The Global Observing System for Climate: Implementation Needs," vol. GCOS-200, ed: GCOS-200, 2016.

[4] S. S. Saatchi, N. L. Harris, S. Brown, M. Lefsky, E. T. A. Mitchard, W. Salas, *et al.*, "Benchmark map of forest carbon stocks in tropical regions across three continents," *Proceedings of the National Academy of Sciences,* vol. 108, pp. 9899-9904, 2011.

[5] J. Holmgren, M. Nilsson, and H. Olsson, "Estimation of tree height and stem volume on plots using airborne laser scanning," *Forest Science,* vol. 49, pp. 419-428, 2003.

[6] N. Labriere, S. Tao, J. Chave, K. Scipal, T. Le Toan, K. Abernethy, *et al.*, "In situ reference datasets from the TropiSAR and AfriSAR campaigns in support of upcoming spaceborne biomass missions," *IEEE Journal of Selected Topics in Applied*

Earth Observations and Remote Sensing, vol. 11, pp. 3617-3627, 2018.

[7] E. Næsset and T. Gobakken, "Estimation of above-and below-ground biomass across regions of the boreal forest zone using airborne laser," *Remote Sensing of Environment,* vol. 112, pp. 3079-3090, 2008.

[8] L. Duncanson, J. R. Kellner, J. Armston, R. Dubayah, D. M. Minor, S. Hancock*, et al.*, "Aboveground biomass density models for NASA's Global Ecosystem Dynamics Investigation (GEDI) lidar mission," *Remote Sensing of Environment,* vol. 270, p. 112845, 2022.

[9] J. R. Kellner, J. Armston, and L. Duncanson, "Algorithm theoretical basis document for GEDI footprint aboveground biomass density," *Earth and Space Science,* vol. 10, p. e2022EA002516, 2023.

[10] R. Nelson, "Modeling forest canopy heights: The effects of canopy shape," *Remote sensing of environment,* vol. 60, pp. 327-334, 1997.

[11] L. Ulander, J. Hagberg, and J. Askne, "ERS-1 SAR interferometry over forested terrain," *EUROPEAN SPACE AGENCY-PUBLICATIONS-ESA SP,* vol. 361, pp. 475-479, 1994.

[12] J. Hagberg, L. M. Ulander, and J. Askne, "Repeat-pass SAR interferometry over forested terrain," *Geoscience and Remote Sensing, IEEE Transactions on,* vol. 33, pp. 331-340, 1995.

[13] J. I. Askne, P. B. Dammert, L. M. Ulander, and G. Smith, "C-band repeat-pass interferometric SAR observations of the forest," *IEEE Transactions on Geoscience and Remote Sensing,* vol. 35, pp. 25-35, 1997.

[14] T. Le Toan, A. Beaudoin, J. Riom, and D. Guyon, "Relating forest biomass to SAR data," *IEEE Transactions on Geoscience and Remote Sensing,* vol. 30, pp. 403-411, 1992.

[15] M. C. Dobson, F. T. Ulaby, T. LeToan, A. Beaudoin, E. S. Kasischke, and N. Christensen, "Dependence of radar backscatter on coniferous forest biomass," *IEEE Transactions on Geoscience and Remote Sensing,* vol. 30, pp. 412-415, 1992.

[16] H. Israelsson, J. Askne, L. M. H. Ulander, P.-O. Frölind, and H. Hellsten, "Forest backscatter mechanisms in CARABAS VHF SAR imagery," in *Int. Symposium on Retrieval of Bio- and Geophysical Parameters from SAR data for Land Applications*, Toulouse, 1995.

[17] M. Santoro, C. Beer, O. Cartus, C. Schmullius, A. Shvidenko, I. McCallum*, et al.*, "Retrieval of growing stock volume in boreal forest using hyper-temporal series of Envisat ASAR ScanSAR backscatter measurements," *Remote Sensing of Environment,* vol. 115, pp. 490-507, 2011.

[18] M. Santoro, O. Cartus, N. Carvalhais, D. M. Rozendaal, V. Avitabile, A. Araza*, et al.*, "The global forest above-ground biomass pool for 2010 estimated from high-resolution satellite observations," *Earth System Science Data,* vol. 13, pp. 3927-3950, 2021.

[19] M. Santoro, O. Cartus, S. Quegan, H. Kay, R. M. Lucas, A. Araza*, et al.*, "Design and performance of the Climate Change Initiative Biomass global retrieval algorithm," *Science of Remote Sensing,* p. 100169, 2024.

[20] M. Werner, "Shuttle radar topography mission (SRTM) mission overview," *Frequenz,* vol. 55, pp. 75-79, 2001.

[21] M. Zink, G. Krieger, H. Fiedler, and A. Moreira, "The TanDEM-X mission: Overview and status," in *2007 IEEE International Geoscience and Remote Sensing Symposium*, 2007, pp. 3944-3947.

[22] R. Treuhaft, F. Gonçalves, J. R. dos Santos, M. Keller, M. Palace, S. N. Madsen*, et al.*, "Tropical-forest biomass estimation at X-band from the spaceborne TanDEM-X interferometer," *IEEE Geoscience and Remote Sensing Letters,* vol. 12, pp. 239-243, 2014.

[23] R. Treuhaft, Y. Lei, F. Goncalves, M. Keller, J. R. d. Santos, M. Neumann*, et al.*, "Tropical-Forest Structure and Biomass Dynamics from TanDEM-X Radar Interferometry," *Forests,* vol. 8, p. 277, 2017.

[24] D. H. T. Minh, T. Le Toan, F. Rocca, S. Tebaldini, M. M. d'Alessandro, and L. Villard, "Relating P-band synthetic aperture radar tomography to tropical forest biomass," *IEEE Transactions on Geoscience and Remote Sensing,* vol. 52, pp. 967-979, 2014.

[25] N. Ramachandran, S. Saatchi, S. Tebaldini, M. M. d'Alessandro, and O. Dikshit, "Mapping tropical forest aboveground biomass using airborne SAR tomography," *Scientific Reports,* vol. 13, p. 6233, 2023

[26] F. Banda, D. Giudici, T. Le Toan, M. Mariotti d´Alessandro, K. Papathanassiou, S. Quegan*, et al.*, "The BIOMASS Level 2 Prototype Processor: Design and Experimental Results of Above-Ground Biomass Estimation," *Remote Sensing,* vol. 12, p. 985, 2020.

[27] M. J. Soja, S. Quegan, M. M. d'Alessandro, F. Banda, K. Scipal, S. Tebaldini*, et al.*, "Mapping above-ground biomass in tropical forests with ground-cancelled P-band SAR and limited reference data," *Remote Sensing of Environment,* vol. 253, p. 112153, 2021.

[28] S. R. Cloude and K. P. Papathanassiou, "Polarimetric SAR interferometry," *IEEE Transactions on Geoscience and Remote Sensing,* vol. 36, pp. 1151-1165, 1998.

[29] K. P. Papathanassiou and S. R. Cloude, "Single-baseline polarimetric SAR interferometry," *IEEE Transactions on Geoscience and Remote Sensing,* vol. 39, pp. 2352-2363, 2001.

[30] P. Rizzoli, M. Martone, C. Gonzalez, C. Wecklich, D. B. Tridon, B. Bräutigam*, et al.*, "Generation and performance assessment of the global TanDEM-X digital elevation model," *ISPRS Journal of Photogrammetry and Remote Sensing,* vol. 132, pp. 119-139, 2017.

[31] B. Wessel, M. Huber, C. Wohlfart, U. Marschalk, D. Kosmann, and A. Roth, "Accuracy assessment of the global TanDEM-X Digital Elevation Model with GPS data," *ISPRS Journal of Photogrammetry and Remote Sensing,* vol. 139, pp. 171-182, 2018.

[32] J. I. Askne, "Relating forest biomass to TanDEM-X mean phase height," *IEEE Journal of Selected Topics in Applied Earth Observations and Remote Sensing,* vol. 18, pp. 24039-24050, 2025.

[33] M. El Hage, L. Villard, L. Ferro-Famil, and L. Polidori, "Potential of the upcoming Biomass P-band radar mission for digital terrain modelling beneath dense tropical forests: first accuracy assessment," *ISPRS Annals of the Photogrammetry, Remote Sensing and Spatial Information Sciences,* vol. 3, pp. 125-130, 2024.

[34] M. M. d'Alessandro and S. Tebaldini, "Retrieval of terrain topography in tropical forests using P-band SAR tomography," in *IGARSS 2018-2018 IEEE International Geoscience and Remote Sensing Symposium*, 2018, pp. 8598-8600.

[35] D. M. Olson, E. Dinerstein, E. D. Wikramanayake, N. D. Burgess, G. V. Powell, E. C. Underwood*, et al.*, "Terrestrial Ecoregions of the World: A New Map of Life on Earth: A new global map of terrestrial ecoregions provides an innovative tool for conserving biodiversity," *BioScience,* vol. 51, pp. 933-938, 2001.

[36] I. Hajnsek, "BIOSAR 2008 Technical Assistance for the Development of Airborne SAR and Geophysical Measurements during the BioSAR 2008 Experiment, Final Report," 2009.

[37] L. M. H. Ulander, A. Gustavsson, P. Dubois-Fernandez, X. Dupuis, J. E. S. Fransson, J. Holmgren*, et al.*, "BIOSAR 2010 - A SAR campaign in support to the BIOMASS mission," presented at the Geoscience and Remote Sensing Symposium (IGARSS), 2011, Vancouver, BC, 2011.

[38] N. Labriere, S. Tao, J. Chave, K. Scipal, T. Le Toan, K. Abernethy*, et al.*, "In situ reference datasets from the TropiSAR and AfriSAR campaigns in support of upcoming spaceborne biomass missions," *IEEE Journal of Selected Topics in Applied Earth Observations and Remote Sensing,* pp. 3617-3627, 2018.

[39] O. Lachenaud, T. Stévart, D. Ikabanga, E. Ngagnia Ndjabouda, and G. Walters, "Les forêts littorales de la région de Libreville (Gabon) et leur importance pour la conservation: description d'un nouveau Psychotria (Rubiaceae) endémique," *Plant Ecology and Evolution,* vol. 146, pp. 68-74, 2013.

[40] M. Lisiewicz, A. Kamińska, B. Kraszewski, Ł. Kuberski, K. Pilch, and K. Stereńczak, "Comprehensive mapping of individual living and dead tree species using leaf-on and leaf-off ALS and CIR data in a complex temperate forest," *Forestry: An International Journal of Forest Research,* p. cpaf007, 2025.

[41] S. Tebaldini, M. M. d'Alessandro, L. M. Ulander, P. Bennet, A. Gustavsson, A. Coccia*, et al.*, "TomoSense: A unique 3D dataset over temperate forest combining multi-frequency mono-and bi-static tomographic SAR with terrestrial, UAV and airborne lidar, and in-situ forest census," *Remote Sensing of Environment,* vol. 290, p. 113532, 2023.

[42] T. Wardlaw, "Measuring a fire. The story of the January 2019 fire told from measurements at the Warra Supersite, Tasmania," *Fire,* vol. 4, p. 15, 2021.

[43] M. Santoro, J. Askne, G. Smith, and J. E. Fransson, "Stem volume retrieval in boreal forests from ERS-1/2 interferometry," *Remote Sensing of Environment,* vol. 81, pp. 19-35, 2002.

[44] J. Askne and L. M. H. Ulander, "Boreal forest properties from TanDEM-X data using interferometric water cloud model and implications for a bistatic C-band mission," *IEEE Journal of Selected Topics in Applied Earth Observations and Remote Sensing,* vol. 14, pp. 8627-8637, 2021.

[45] J. I. H. Askne, H. J. Persson, and L. M. H. Ulander, "On the Sensitivity of TanDEM-X-Observations to Boreal Forest Structure," *Remote Sensing,* vol. 11, p. 1644, 2019.

[46] M. J. Soja, H. J. Persson, and L. M. H. Ulander, "Estimation of forest biomass from two-level model inversion of single-pass InSAR data," *IEEE Transactions on Geoscience and Remote Sensing,* vol. 53, pp. 5083-5099, 2015.

[47] J. I. Askne, J. E. Fransson, M. Santoro, M. J. Soja, and L. M. Ulander, "Model-based biomass estimation of a hemi-boreal forest from multitemporal TanDEM-X acquisitions," *Remote Sensing,* vol. 5, pp. 5574-5597, 2013.

[48] J. I. H. Askne, M. J. Soja, and L. M. H. Ulander, "Biomass estimation in a boreal forest from TanDEM-X data, lidar DTM, and the interferometric water cloud model," *Remote Sensing of Environment,* vol. 196, pp. 265-278, 2017.

[49] J. I. H. Askne, J. E. S. Fransson, M. Santoro, M. J. Soja, and L. M. H. Ulander, "Model-based biomass estimation of a hemi-boreal forest from multitemporal TanDEM-X acquisitions," *Remote Sensing,* vol. 5, pp. 5574-5597, 2013.

[50] N. Knapp, R. Fischer, V. Cazcarra-Bes, and A. Huth, "Structure metrics to generalize biomass estimation from lidar across forest types from different continents," *Remote Sensing of Environment,* vol. 237, p. 111597, 2020.

[51] T. Mette, K. P. Papathanassiou, I. Hajnsek, and R. Zimmermann, "Forest Biomass Estimation using Polarimetric SAR Interferometry," in *Workshop on POLinSAR - Applications of SAR Polarimetry and Polarimetric Interferometry*, Frascati, Italy, 2003.

[52] S. Solberg, R. Astrup, J. Breidenbach, B. Nilsen, and D. Weydahl, "Monitoring spruce volume and biomass with InSAR data from TanDEM-X," *Remote Sensing of Environment,* vol. 139, pp. 60-67, 2013.

[53] R. N. Treuhaft and P. R. Siqueira, "The calculated performance of forest structure and biomass estimates from interferometric radar," *Waves in Random Media,* vol. 14, pp. S345-S358, 2004.

[54] M. Hunter, M. Keller, D. Victoria, and D. C. Morton, "Tree height and tropical forest biomass estimation," *Biogeosciences,* vol. 10, pp. 8385-8399, 2013.

[55] X. Wu, X. Wang, Y. Wu, X. Xia, and J. Fang, "Forest biomass is strongly shaped by forest height across boreal to tropical forests in China," *Journal of Plant Ecology,* vol. 8, pp. 559-567, 2015.

[56] J. Wan, C. Wang, P. Shen, and Y. Wei, "An Improved Sparse Bayesian Learning SAR Tomography Method and Its Application for Forest Vertical Structure Inversion," *IEEE Journal of Selected Topics in Applied Earth Observations and Remote Sensing,* 2025.

[57] J. I. H. Askne, H. J. Persson, and L. M. H. Ulander, "Biomass Growth from Multi-Temporal TanDEM-X Interferometric Synthetic Aperture Radar Observations of a Boreal Forest Site," *Remote Sensing,* vol. 10, p. 603, 2018.

[58] J. Chave, M. Réjou-Méchain, A. Búrquez, E. Chidumayo, M. S. Colgan, W. B. Delitti*, et al.*, "Improved allometric models to estimate the aboveground biomass of tropical trees," *Global change biology,* vol. 20, pp. 3177-3190, 2014.

[59] L. Mo, T. W. Crowther, D. S. Maynard, J. Van den Hoogen, H. Ma, L. Bialic-Murphy*, et al.*, "The global distribution and drivers of wood density and their impact on forest carbon stocks," *Nature Ecology & Evolution,* vol. 8, pp. 2195-2212, 2024.

Jan I. H. Askne (Life Fellow, IEEE) was born in Lund, Sweden. He has been active with Chalmers University of Technology, Göteborg, Sweden, in 1961 and a Professor from 1984 to 2001 until retirement. Prof. Askne has been a Member of the Remote Sensing Committee of the Swedish National Space Board, ESA EOPAG (for ERS-1 and 2), ESA ENVISAT Science Advisory Group on ASAR, and EARSeL committees. He has been involved in a number of international courses on microwave remote sensing and has been the local organizer for International Symposium on Microwave Signatures in Remote Sensing in 1987, the 14th EARSeL Symposium in 1994, and the ESA ERS Envisat Symposium 2000, all in Göteborg. He started with projects on wave propagation (in the troposphere, ionosphere, and magnetosphere, plasma, and quantum media) and in radio astronomy (radiation from molecules in cosmic clouds). He shifted in the seventies to work on passive remote sensing (oil spill, meteorological parameters in the troposphere, and ozone in the stratosphere), and later on active remote sensing (sea ice and forestry). Since retirement, his interests have concentrated on interferometric SAR related to forestry. He was the recipient of the Thulin Medal in silver from the Swedish Society of Aeronautics and Astronautics "for important contributions as Scientist and Educator within Swedish and International Remote Sensing," in 2004.